GROUND-MOTION RELATIONS FOR EARTHQUAKES IN THE PACIFIC NORTHWEST: CRUSTAL, IN-SLAB AND OFFSHORE EVENTS

Gail M. Atkinson
Dept. Earth Sciences, Carleton University
Ottawa, Ontario K1A 5B6
613-623-3240 (phone/fax)
gmatkinson@aol.com

Final Technical Report:
USGS Award 03HQGR0081
July 22, 2004

Ground-Motion Relations for Earthquakes in the Pacific Northwest: Crustal, In-Slab and Offshore Events

Gail M. Atkinson

Final Technical Report: USGS Award 03HQGR0081. July 22, 2004

ABSTRACT

Regional ground motion generation and propagation must be characterized in order to adequately assess seismic hazard. In the Cascadia region of southwestern British Columbia and northwestern Washington, the ground-motion issues are particularly complex due to the contributions to hazard from four distinct types of events, all of which behave differently in terms of their ground motion propagation characteristics: (i) shallow earthquakes occurring in the continental crust; (ii) shallow earthquakes occurring offshore in oceanic crust; (iii) earthquakes occurring within the subducting Juan de Fuca slab beneath the continent; and (iv) great subduction earthquakes on the interface between the subducting Juan de Fuca plate and the overriding North American plate. In this study, empirical data recorded within the Cascadia region are used to examine the source and attenuation characteristics of ground motion amplitudes from the first three of these event types (crustal, offshore, in-slab), and thereby develop regional ground-motion relations.

A simple application of the hybrid-empirical approach is well-suited to the development of regional ground-motion relations for earthquakes in the Cascadia region. Separate ground-motion relations are required to characterize crustal, in-slab and offshore events. For crustal earthquakes in Cascadia, ground motions are obtained by multiplying California ground-motion relations by a frequency-dependent factor to account for regional differences in crustal amplification. The ground motion from offshore events can be predicted by using the Cascadia crustal relations, but for one-half moment magnitude unit less (eg. predict **M**7 motions using relations for **M**6.5). In-slab earthquakes attenuate more rapidly with distance than do crustal earthquakes. Their ground motions are predicted by multiplying Cascadia crustal relations by the factor 1.17 exp(-0.004 R) (where R is distance). The developed ground-motion relations for Cascadia earthquakes are in reasonable agreement with recorded ground motions in the region. The proposed relations are the first region-specific ground-motion relations to be developed for use in seismic hazard analysis in the Cascadia region.

INTRODUCTION

There is growing recognition of the earthquake hazard from both crustal and subduction earthquakes in the Cascadia region of southwestern British Columbia and northwestern Washington. A priority task to enable reliable seismic hazard estimation for the region is the development of region-specific ground motion relations, which predict average ground motion amplitudes (response spectra and peak ground acceleration and velocity) as simple functions of earthquake magnitude (moment magnitude, **M**), event type (eg. crustal or in-slab), and distance. At present, national

seismic hazard maps are based on the assumption that ground motions from shallow crustal events in Cascadia may be predicted using empirical ground motion relations developed for California, while ground motions from large subduction events (interface and in-slab) may be predicted based on empirical relations developed from a global subduction database (eg. Frankel et al., 1996, 1999; Adams and Halchuk, 2003). These assumptions were born more of necessity than knowledge, and should be critically evaluated using regional ground motion data. It is important to understand regional differences in ground-motion generation and propagation, and differences between event types within the region, in order to adequately assess seismic hazard. In the Cascadia region, the situation is particularly complex due to the contributions to hazard from four distinct types of events, all of which behave differently in terms of their ground motion propagation characteristics (Ristau et al., 2003): (i) shallow earthquakes occurring in the continental crust; (ii) shallow earthquakes occurring offshore in oceanic crust; (iii) earthquakes occurring within the subducting Juan de Fuca slab beneath the continent; and (iv) great subduction earthquakes on the interface between the subducting Juan de Fuca plate and the overriding North American plate.

The purpose of this study is to use empirical data recorded within the Cascadia region to examine the source and attenuation characteristics of ground motion amplitudes from the first three of these event types (crustal, offshore, in-slab), and thereby develop regional ground-motion relations. Subduction events on the interface are not addressed in this paper because there are no empirical data from Cascadia for this event type; for interface events, we are forced to rely on inferences from the global database (eg. Atkinson and Boore, 2003; Youngs et al., 1997). The approach taken in this study is to use the results of empirical analyses of Cascadia data to formulate the basic assumptions required to develop regional ground motion relations for crustal, offshore and in-slab earthquakes, following the hybrid-empirical approach (Campbell, 2003; Atkinson, 2001). The hybrid-empirical approach was adopted because the analyses of the source and attenuation characteristics in Cascadia suggested that this method was ideally suited to this application; simple modifications to California ground motion relations can be employed to develop separate relations for crustal, in-slab and offshore earthquakes in the Cascadia region. The ground-motion relations developed by this approach are validated using response spectra from regional earthquakes of moment magnitude (**M**) ≥4 at distances up to 300 km.

GROUND MOTION DATABASE

The ground-motion database for the Cascadia region has been growing steadily over the last decade, due to increased numbers of broadband seismographic and strong-motion instruments and the occurrence of a few strong earthquakes such as the **M** 6.8 Nisqually, Washington earthquake in 2000; however the empirical database is still dominated by small to moderate events (**M**<6), especially in the case of crustal earthquakes. The seismographic database includes older short-period vertical-component data recorded in the 1980's and early 1990's, along with 3-component broadband data recorded mostly within the last 5 years. Broadband seismographic data were collected from the Canadian National Seismographic Network (CNSN) and the U.S. National Seismographic Network (USNSN) via their automatic data request management tools (autodrm); older short-period data were compiled by Atkinson (1995). Strong-motion

data have been collected for a few moderate-to-large events, most notably the Nisqually event (data from compilation of Atkinson and Boore, 2003). Figure 1 shows the location of study events, while Figure 2 shows the distribution of seismographic data compiled for this study in magnitude and distance. The distance measure is hypocentral distance, which is appropriate for the small magnitudes that dominate the data. In-slab events were distinguished from crustal or offshore events based on focal depth, combined with geographic location and information on structure from the geophysical profiling of Hyndman et al. (1996). All of the events deeper than 30 km within our dataset likely occurred within the subducting slab. Events with intermediate depths (20 to 30 km) were examined individually to determine whether they are crustal or in-slab (based on their location and depth). Shallow events are either crustal continental events or offshore events, depending on their location.

Not all of the data points plotted on Figure 2 represent broad-band three-component data. Of the total database of over 15,000 records, about 1000 are short-period vertical-component. The short-period records make up about 10% of the 5000 records for M>4 events, but of the limited dataset for shallow crustal earthquakes, most of the records are short-period (800 vertical components, 400 horizontal-components). The short-period vertical-component records are thus particularly important for the shallow crustal earthquakes. Almost all of the records considered in this study were recorded on hard-rock sites (NEHRP site class A or B), except for a few hundred soil recordings, most of which were from the Nisqually earthquake. Note that the distribution of data with distance is generally good beyond 40 km, but poor at closer distances. This places significant constraints on the use the empirical database in ground-motion studies.

The seismographic data were processed as described by Atkinson and Mereu (1992) and Atkinson (2004). Briefly, for each record, the window of strongest shaking (shear window, including direct, reflected and refracted phases) was selected, and a 5% taper was applied at each end of the window. The Fourier spectrum of acceleration was determined, correcting for instrument response. The spectra were smoothed and tabulated over increments of 0.1 log frequency units, for log frequencies of -1 to 1.3 (eg. 0.1 to 20 Hz) where available. Spectra for a pre-event noise window, normalized to the same duration as the signal window, were processed and tabulated in the same manner. Data were retained for further analysis only at frequencies for which the signal-to-noise ratio exceeds two. Finally, the compiled Fourier spectral data were checked to eliminate data in magnitude-distance ranges affected by low-amplitude 'quantization noise' problems (Atkinson, 2004). The main use of the Fourier amplitude spectral database is in investigation of the source and attenuation characteristics of the events. To focus on these effects, Fourier spectral data were compiled only for hard-rock sites. Data over the range of magnitudes and distances shown in Figure 2 were considered.

To compile a response spectra database to be used later in validation of ground-motion relations, both rock and soil observations were compiled for events of **M**≥4 at distances up to 300 km. Response spectra (pseudo-acceleration) were computed for 5% damping from the corrected acceleration records. Table 1 lists the events for which response spectra data were compiled. Moment magnitudes are from Ristau (2004) for most events, or from published values for large events (Atkinson and Boore, 2003). For a few of the smallest events, moment magnitude was estimated from m1 as described later

in the paper. Both vertical and horizontal components were compiled. There are 835 records in the response spectral database, 643 of which were recorded on rock.

ATTENUATION AND SOURCE CHARACTERISTICS OF CASCADIA EARTHQUAKES

Regression analysis of the Fourier amplitude spectra is used to determine the attenuation characteristics of crustal, in-slab and offshore events and infer the gross characteristics of their source radiation. Regression is performed by the maximum likelihood method using the algorithm of Joyner and Boore (1993, 1994). Because of the wealth of vertical-component data and their predominance for the shallow crustal earthquake dataset, the regressions initially focus on the vertical component. The horizontal component is addressed later by examining the residuals obtained when the vertical-component regression equation is used to predict the horizontal-component amplitudes.

Initial inspection of the data indicates that the three data types exhibit distinct attenuation characteristics and thus need to be regressed separately. This can be seen in Figure 3, which shows a plot of amplitudes versus distance for a subset of the data having catalog magnitude 3.0 to 3.5 (where the catalog magnitude is generally ML for crustal and in-slab events, and mb for offshore events). Ristau et al. (2003) have noted that offshore events do not propagate efficiently into the continental crust, and therefore have reduced amplitudes, and reduced catalog magnitudes, relative to crustal events of the same moment magnitude. Thus the offshore events plotted on Figure 3 would actually be associated with a larger moment magnitude (as much as 1 unit larger) than the crustal or in-slab events in the figure. Several interesting features can be observed on Figure 3. The crustal events have a distinct attenuation shape that suggests a trilinear attenuation form similar to that noted in eastern North America by Atkinson and Mereu (1992) and Atkinson (2004). The trilinear form represents direct-wave attenuation to about 100 km, followed by a flattening, most likely due to post-critical reflections and refractions from the Moho and other internal discontinuities (Burger et al., 1987). At distances beyond about 200 km, the signal is dominated by the Lg phase, consisting of multiply reflected and refracted shear waves (Ristau et al., 2004). The attenuation behavior varies with distance according to these arrivals. There may also be a transition zone in attenuation behavior for in-slab and offshore events, though it is not seen as strongly for these events. At large distances, beyond about 250 km, the attenuation rate appears the same for all three types of events. At large distances, the signal consists of multiple reflections and refractions traveling in the crustal waveguide, and will attenuate similarly regardless of the origin of the source (Ristau et al., 2003).

For each dataset (vertical components for crustal, in-slab, offshore events) I fit the observed Fourier amplitudes at each frequency to an equation of the general form:

$$\log A_{ij} = c_1 + c_2 (M_i\text{-}4) + c_3 (M_i\text{-}4)^2 \; - b \log R_{ij} - c_4 R_{ij} \qquad (1)$$

where $A_{if=}$ is the observed spectral amplitude of earthquake i at station j, R_{ij} is hypocentral distance, b is the geometric spreading coefficient, and c_1 through c_4 are the other coefficients to be determined. M is a magnitude measure. The most commonly available magnitude for the events from the earthquake catalogs is ML for the crustal events, and mb for the offshore events. But the catalog contains a mixture of magnitudes,

including also MS for some of the larger events, and Mc (coda magnitude) for some of the crustal events in Washington. The optimal magnitude measure is moment magnitude (**M)** but this is available only for the larger events (M>4) since 1995 (Ristau, 2004), plus a few large older events. I therefore follow the approach taken in Atkinson (2004) and use the intermediate spectral magnitude measure m1 (Chen and Atkinson, 2002) as the predictive magnitude variable in the regressions to determine the attenuation characteristics. I choose m1 because it is simple to determine from the data, and provides a uniform characterization of overall amplitude level for all events on a common scale. In most regions, m1 has been shown to be a good estimate of **M** for moderate events (Chen and Atkinson, 2002; Atkinson, 2004; Motazedian and Atkinson, 2004). The relationship between m1 and **M** is examined later for events with known moment magnitude.

The magnitude m1 is defined from the average 1-Hz Fourier acceleration amplitude at a reference distance of 10 km (Chen and Atkinson, 2002). Thus we need to know the attenuation model, in order to correct observations back to the reference distance of 10 km and obtain m1 for each event as an average of values over all records. This can be done iteratively, to determine both the attenuation model and the m1 values. I begin with the catalog magnitudes as initial estimates of m1, and perform a preliminary regression for the 1-Hz amplitudes to Equation (1), assuming a single *b* value of 1.0 over all distances, and determining the best value of c_4 for each dataset (crustal, in-slab, offshore). This crude initial attenuation model can then be used to correct all amplitudes to 10 km, and provide a reasonable estimate of m1 for each event. In the regressions that follow, the m1 estimates will be refined to be consistent with the detailed attenuation model that is determined for each dataset.

The next stage of the regression exploits the observation that the attenuation rate is common to all event types at large distances. I assume that attenuation beyond 250 km for all events can be modeled by Equation (1) with b=0.5, corresponding to surface-wave spreading in a half-space. The anelastic coefficient, c_4, is inversely related to the quality factor, Q:

$$Q = (\pi f) / (\ln (10)\, c_4\, \beta) \qquad (2)$$

where β is the shear-wave velocity (eg. Atkinson and Mereu, 1992). I regress the Fourier spectral amplitudes for just the observations beyond 250 km to determine the coefficient c4 (values plotted in Figure 5). By Equation (2), the regional Quality factor (between approximately 0.5 and 15 Hz) is given by:

$$Q = 229\ f^{0.60} \qquad (3)$$

With the distant attenuation established, I then look in detail at the attenuation for the crustal, in-slab and offshore datasets separately. I apply Equation (2), allowing the coefficient *b* to take on different values in different distance ranges, to accommodate the geometric attenuation behavior of the shear window as different phases arrive. A hinged trilinear form with transitions at distances $rt_1$and rt_2 is assumed. The regression determines the best value for the attenuation slope *b* in the distance range from $R \leq rt_1$, the best value of the slope at $rt_1 < R \leq rt_2$ (the value of the attenuation slope in the transition zone is denoted *t* to avoid confusion with *b*) and the values for the transition distances $rt_1$and rt_2. In all cases the attenuation beyond the distance rt_2 is assumed to be given by a

slope of 0.5, with the fixed c_4 values determined in the first step (and shown in Figure 5). The solution is the set of values that minimizes the average total error, where the error of each observation is measured as the absolute value of the observed log amplitude minus the predicted log amplitude. Note that this scheme covers the possibility of a hinged bilinear model (single transition distance) as well as the hinged trilinear model; for a bilinear model, the solution would indicate that the two transition distances were close together, or that the slopes *b* and *t* were similar.

Initial regressions indicated that the observed attenuation is complex for each dataset, probably due to the complicated crustal and subcrustal structure in the region. In order to obtain a satisfactory fit to the data at all frequencies and distances, it is necessary to allow all attenuation coefficients to be frequency-dependent (but the transition distances are constrained to be the same over all frequencies). Within the crustal dataset, the effect of focal depth on the attenuation residuals was investigated, but found to be not significant. Thus it is not necessary to consider focal depth as an additional predictive variable.

For each dataset, after regression to determine the coefficient values, the m1 values were re-evaluated using the obtained attenuation model, then the regressions repeated with the new m1 values. This process was repeated until there were no further changes to the attenuation coefficients or m1 values; m1 values converge rapidly, with only a few iterations required. The final attenuation model, presented in the next section, provides an excellent distribution of residuals over all distances and all frequencies. This is illustrated for the crustal earthquakes at a frequency of 2 Hz in Figure 4.

Attenuation Results

The attenuation coefficients determined by regression are plotted versus frequency in Figure 5. The values of all coefficients are provided in Table 2. The coefficients can only be determined for frequencies ≥0.5 Hz, due to the paucity of data at lower frequencies. Note that the attenuation coefficients vary significantly between event types, as do the transition distances. However, within a given distance range the net attenuation is not necessarily distinguishable between event types, due to the interplay between coefficients. A trilinear form is required for all datasets to obtain a good fit over the large distance range covered.

To examine the applicability of the attenuation model to the horizontal components, the residuals of the horizontal component motions, when predicted by the vertical-component equation coefficients of Table 2, are computed (as in Atkinson, 2004). These residuals are the H/V (horizontal-to-vertical) ratio. The H/V ratio calculated from the regression residuals depends on frequency, but not on distance. The residuals for each frequency, when regressed against distance, show no significant trend. This indicates that the vertical-component attenuation model also applies to the horizontal component; all this is required is to multiply the vertical-component predictions by the H/V ratio. The H/V ratio is shown versus frequency in Figure 6, and given by:

$$\text{Log H/V} = 0.0566 + 0.0723 \log f \qquad (4)$$

Note that this H/V ratio applies to hard-rock sites only. H/V is generally believed to be a good, if crude, estimate of site response, as discussed by Lermo and Chavez-Garcia (1993), Siddiqqi and Atkinson (2002), Atkinson and Cassidy (2000) and Beresnev and Atkinson (1997). The H/V ratios obtained in this study are consistent with previous results for the region (Siddiqqi and Atkinson, 2002) and conform to the values expected for near-surface shear-wave velocities of about 1.5 km/s (Atkinson and Cassidy, 2000).

Near-Source Spectral Amplitudes

The database is sparse in the near-source region (Figure 2). This, combined with the complex frequency-dependent attenuation observed at regional distances, means that we cannot use the regression results to reliably define source characteristics of the radiation. However, we can use the regression results to define the average Fourier spectra at a reference distance of 40 km – this is about as close to the source as we can get given our data distribution. The use of spectra at a reference distance of 40 km follows the approach advocated by Raoof et al. (1999) and Herrmann and Malagnini (2004) in using regional data to infer source characteristics. The idea is to estimate the spectra at the closest distance that can be obtained reliably, then compare the spectra at that distance to the implications of model predictions.

For each event in the database, we use the attenuation model for that event type (Figure 5) to project the recorded spectrum back to the reference distance of 40 km:

$$\log A40_{ij} = \log A_{ij} + b \log R_{ij} + c_4 R_{ij} \qquad R_{ij} \le r_{t1}$$

$$\log A40_{ij} = \log A_{ij} + b \log r_{t1} + t \log(R_{ij}/r_{t1}) + c_4 R_{ij} \qquad r_{t1} < R_{ij} \le r_{t2}$$

$$\log A40_{ij} = \log A_{ij} + + b \log r_{t1} + t \log(r_{t2}/r_{t1}) + 0.5 \log(R_{ij}/r_{t2}) + c_4 R_{ij} \qquad R_{ij} > r_{t2} \qquad (5)$$

An average of log spectra is then taken over all N_i stations to obtain the event spectrum at the reference distance of 40 km:

$$\log A40_i = \sum_{j=1}^{N_i} \log A40_{ij} / N_i \qquad (6)$$

Figure 7 compares the reference spectra at 40 km for selected events of **M** 4.5 to 6 with standard 100-bar Brune model spectra at 40 km for **M** 4.5, 5, 5.5 and 6, where the Brune model spectrum is given by (Brune, 1970; Boore, 1983):

$$A_{ij}(f) = C M_0 (2\pi f)^2 / [R (1+(f/f_0)^2)] \qquad (7)$$

where M_0 is seismic moment, f_0 is corner frequency, and R is distance (=40km). The constant $C = \Re^{\theta\varphi} F V / (4\pi\rho\beta^3)$, where $\Re^{\theta\varphi}$ = radiation pattern (average value of 0.55 for shear waves), F= free surface amplification (2.0), V= partition onto two horizontal components (0.71), ρ= density (2.8 g/cm^3) and β is shear wave velocity (3.7 km/s). Corner frequency is given by $f_0 = 4.9e+6\, \beta\, (\Delta\sigma / M_0)^{1/3}$ where $\Delta\sigma$ is stress drop in bars, M_0 is in dyne-cm and β is in km/s (Boore, 1983). In making this comparison, I assume that the vertical-component spectrum is equivalent to the random horizontal-component spectrum before any amplification by the regional velocity gradient or near-surface

materials (where the observed H/V ratio represents this amplification). Under this assumption, it is appropriate to compare the vertical-component spectra with an unamplified Brune model for the horizontal component, as per Equation (7). The Brune model is often used in ground-motion modeling as a simple predictive model for source radiation. Note the implicit assumption of simple R^{-1} attenuation from the source to 40 km, corresponding to body-wave spreading in a whole-space. It is not known if this attenuation is applicable, although is seems reasonable to assume that the radiation decays in a simple manner close to the source, before regional crustal structure causes the complexities observed in the regional decay rates. From Figure 7, it can be inferred that moderate crustal and in-slab events are consistent with stress drops of the order of 100 bars. However there is much uncertainty in interpreting source parameters from these comparisons due to the complicated attenuation. The lack of smoothness in the obtained spectral shapes at 40 km partly reflect the frequency-dependence of the attenuation coefficients; the obtained shapes would look slightly different at a different selected reference distance.

Figure 8 compares the m1 magnitude values determined in this study to moment magnitudes determined from regional modeling of the long-period waves, as derived by Ristau (2004). The relationship m1 = **M** appears reasonable for the crustal events and most of the in-slab events. The offshore events, and some of the in-slab events, exhibit a different relationship. For the offshore events, **M** – m1 = 0.9 on average. This is consistent with findings of previous studies of Ristau et al. (2003) and Atkinson and McCartney (2004), which suggest that regional magnitude approximately equals moment magnitude for continental earthquakes, but greatly underestimates moment magnitude for offshore events.

As a check on the sensitivity of the reference near-source spectra at 40 km to the attenuation model, the regressions were repeated using just the data within 200 km of the source, along with a simpler functional form. In this simpler model, the data for each set were fit to Equation (1) assuming a single frequency-independent value of *b*, and allowing the regression to find the best corresponding value of c_4 for each frequency (with separate value of *b* and c_4 for each event type). This approach provides a reasonable fit to the data at intermediate frequencies and for distances less than 200 km, but cannot provide trend-free residuals versus distance at all frequencies. Under this simpler model, the attenuation slope *b* is -1.3 for crustal events, -1.6 for in-slab events, and -0.5 for offshore events with associated c_4 values of 0, 0 and -0.0023, respectively, at 1 Hz, decreasing with increasing frequency to -0.0021, -0.0035 and -0.0083 at 10 Hz. The shallow attenuation slope indicated by the *b* coefficient for offshore events might appear to suggest surface-wave spreading for distances less than 200 km, while the attenuation of in-slab events and crustal events is faster than for direct-wave spreading. However, the *b* coefficients are somewhat misleading, because the high c_4 values obtained under this model for the offshore events must be considered in assessing the overall attenuation. The net attenuation for the offshore events within the first 200 km is not greatly different than that for the crustal events, but the in-slab attenuation is clearly steeper.

Despite a significantly different attenuation model, the inferred spectra at the reference distance of 40 km are consistent with our previous estimates, generally

matching these amplitudes to within about 0.1 log units. This suggests that the reference spectra at 40 km are reliable, and not overly sensitive to the attenuation model. The same would not be true if the spectra were extrapolated all the way back to the source, beyond the range where the amplitudes are constrained by the data. This is why the definition of near-source spectra at a reference distance of 40 km is a good approach; it results in well-constrained spectra that are not overly sensitive to the adopted form of the attenuation model. In summary, spectra can be obtained from the data at a reference distance of 40 km to within an uncertainty of about 0.1 log units (factor of 1.3), but the use of these spectra to infer source characteristics is subject to significant uncertainty as the attenuation from the source to 40 km is not well understood.

Comparison of Near-Source Spectra for Cascadia versus California

It is useful to know how near-source spectra for earthquakes in Cascadia compare with the better-instrumented shallow California earthquakes. Atkinson and Silva (1997) performed regression analysis of the empirical California strong-motion database to obtain a model of the attenuation of Fourier spectral amplitudes. Their results can be used directly to obtain Fourier spectra of well-recorded California earthquake at the reference distance of 40 km, for comparison with the events of this study. In making the comparisons, differences between typical site conditions in the two regions must be considered. The Atkinson and Silva (1997) spectra are for motions recorded on soft rock California sites of NEHRP C category (shear-wave velocity about 620 m/s), whereas our spectra are for hard-rock sites of NEHRP A/B category (shear-wave velocity about 1500 m/s). The fact that the Cascadia region was glaciated in recent history, while California was not, has a significant but predictable influence on average site response for "rock" sites; California rock is not equivalent to Cascadia rock. The amplification factors that apply to typical California soft rock sites have been evaluated by Boore and Joyner (1997). They provide frequency-dependent factors that represent the amplification of motions through the crustal velocity gradient (from 3.6 km/s at source depths to 620 m/s at the surface), combined with near-surface attenuation due to the "kappa" operator (where $\kappa = 0.035$). I adopt their generic soft-rock factors as an estimate of regional site amplification for horizontal-component Fourier spectra recorded on NEHRP C sites in California. Accordingly, I divide the horizontal-component spectra obtained by Atkinson and Silva (1997) for each event, at a reference distance of 40 km, by these factors (listed as FC(CA) in Table 3) to obtain the equivalent unamplified motions. For Cascadia, the reference spectra at 40 km are vertical-component spectra. As mentioned above, I assume that vertical-component spectra equal the horizontal-component spectra before amplification through the shear-wave velocity profile; in other words, I assume that the H/V ratio represents regional site amplification for hard-rock sites in Cascadia. This assumption follows the work of Lermo and Chavez-Garcia (1993) and is supported for rock sites by Beresnev and Atkinson (1997) and Atkinson and Cassidy (2000). Under this assumption, the reference vertical-component spectra for Cascadia can be directly compared to the California reference spectra, divided by California site amplification factors.

Figure 9 shows the results of this comparison at four spectral frequencies. In making this plot, the moment magnitude values of Ristau (2004) were used for Cascadia events where available (Ristau's estimates are available for most of the **M**>4 events). For

smaller events with no moment magnitude estimate, I assumed that **M** = m1 for crustal and in-slab events, and that **M** = m1+0.9 for offshore events. Unfortunately, the magnitude-range of overlap between the studies is limited. Nevertheless the figure supports the hypothesis that Cascadia source parameters for shallow crustal events are approximately equal to (or perhaps slightly less than) California source parameters for shallow crustal events. Perhaps surprisingly, the in-slab source parameters also appear to follow the California trend. The offshore events have significantly lower source spectral amplitudes than do the California crustal events, with an offset of about 0.5 to 1 magnitude units. The offset appears to be largest at small magnitudes and diminish with increasing magnitude, but the data are weak. Note that this offset is fully consistent with the finding that m1 values are about 0.5 to 1 units lower than moment magnitude values. As a generalization, it appears that the near-source amplitudes of offshore events could be predicted by using a California crustal event about 0.5 moment magnitude units lower (eg. California **M**6 is equivalent to offshore **M**6.5).

GROUND-MOTION RELATIONS FOR CASCADIA

The apparent similarity of near-source amplitudes for crustal and in-slab earthquakes in Cascadia with those of California earthquakes suggests that ground-motion relations for Cascadia earthquakes can be developed using a simple hybrid-empirical approach. The hybrid-empirical approach adjusts empirical ground-motion relations that have been validated for California to be applicable to other regions, by applying factors that account for known regional differences (Campbell, 2003; Atkinson, 2001). For crustal and in-slab events, all that is required is to account for differences in regional crustal amplification effects (as discussed above), and for any differences in attenuation rates. We can follow the simple approach based on multiplicative factors, as outlined by Atkinson (2001), which works well when there are no differences in source characteristics. This differs from the Campbell (2003) approach, which uses simulations based on a stochastic model to determine the adjustment factors; the Campbell approach is more general and can more readily handle differences in source spectra, at the cost of additional complexity in application. For the offshore events, we can also use the simple approach and adjust for the source differences by using an offset of 0.5 magnitude units (ie. use **M**=6.5 to predict ground motions for an offshore event of **M**=7). A hybrid-empirical approach is ideally suited for Cascadia because it will result in ground-motion relations that have a simple relationship to their California counterparts. The approach mitigates the observed complexities in attenuation that are difficult to fully model with our limited data, but can be treated approximately with the hybrid empirical approach.

To apply the hybrid-empirical method in its simplest form, as proposed by Atkinson (2001), we must develop adjustment factors to apply to California relations to account for: (i) regional crustal amplification and (ii) attenuation differences between the two regions. To consider differences in crustal amplification, as discussed above we can assume that the amplification for California soft-rock (NEHRP C) sites is given for horizontal components by the generic California rock amplification factors of Boore and Joyner (1997), with κ=0.035. These factors are listed in the column FC(CA) of Table 3. In Cascadia, we assume that the regional amplification for the horizontal component on hard-rock sites (NEHRP A/B) is given by the regional H/V ratio, with κ=0.011 (Atkinson, 1995). These factors are listed in column FC(BC) of Table 3. The relative

amplification factor, to apply to California rock relations to predict motions on hard rock in Cascadia, is FC(BC)/FC(CA), as given in Table 3. Note that the reference rock condition is different for the two regions. For soil sites in Cascadia, we can apply the generic soil factors from an empirical California ground-motion relation to predict soil motions from the hard-rock motions. For this purpose, I adopt the soil response terms in the Abrahamson and Silva (1997) ground-motion relations.

The effects of regional differences in attenuation are examined in Figure 10. Figure 10 plots the relative attenuation of Fourier amplitudes in California (from Atkinson and Silva, 1997) in comparison to that for events in Cascadia, beyond the reference distance of 40 km, using the frequency-dependent attenuation model developed in this study. It is observed that overall differences in attenuation of crustal earthquakes between California and Cascadia are small enough to be neglected within the first 200 km. This is the distance range of interest for the development of ground-motion relations for seismic hazard applications. The offshore attenuation is also sufficiently similar to the crustal attenuation within 200 km to neglect the differences. However, note the offshore attenuation is steeper at greater distances as seen in Figure 3; also keep in mind that this is only relative attenuation, not overall amplitudes for a given **M**. In-slab events attenuate noticeably faster than California events. The effect can be modeled with the multiplicative attenuation factor FA(slab) = 1.17 exp(-0.004 R). This factor has the value 1.0 at 40 km, decreasing to 0.52 at 200 km.

I apply the factors outlined above and given in Table 3 to selected California ground-motion relations to obtain the predicted relations for Cascadia, as follows:

1. For crustal earthquakes: Multiply California relations by factor FC(BC)/FC(CA).
2. For in-slab earthquakes: Multiply California relations by factor FC(BC)/FC(CA) * 1.17 exp(-0.004R).
3. For offshore earthquakes: Multiply California relations for 0.5 **M** unit greater than target magnitude by the factor FC(BC)/FC(CA). (Note: In practice, this offset is counterbalanced by the common convention that assumes **M** = ML for such events, when the actual relation is closer to **M** = ML + 0.7 (Ristau et al., 2003; Atkinson and McCartney, 2004). Thus the common miscalculation of magnitude for offshore events results in predicting lower ground motions, which is equivalent to the approach taken here).

The selected California relations are the empirical relations of Abrahamson and Silva (1997) and the empirical-stochastic relations of Atkinson and Silva (2000). The Atkinson and Silva (2000) relations make a useful comparison as they are referenced to a simple model of source and attenuation, and are applicable to somewhat lower magnitudes and larger distances than strictly-empirical relations.

The developed horizontal-component ground-motion relations for Cascadia events can be compared to response spectra data (PSA, 5% damped pseudo-acceleration), as listed in Table 1. Both horizontal and vertical-component data may be used in these comparisons, provided vertical-component data are multiplied by the H/V ratio (Equation 4). Figure 11 shows an example comparison for events of **M** 4 to 5 on rock sites, for crustal and in-slab events. The relations overestimate PSA overall, but the shape of the

attenuation is appropriate. It is seen that vertical-component data (*H/V) and the horizontal-component data are consistent with each other. The modified Abrahamson and Silva (1997) and the modified Atkinson and Silva (2000) relations are very similar to each other. This is true at larger magnitudes also (Atkinson and Silva, 2000). However the Atkinson and Silva (2000) relations have a slightly better attenuation shape with distance, in terms of matching the attenuation shape exhibited by the data. Therefore in the comparisons that follow I will focus on the modified Atkinson and Silva (2000) relations. For ease of use, the modified relations (after multiplication by the Cascadia factors) have been refit to a standard equation of the form:

$$\text{Log } Y = a_1 + a_2 (\mathbf{M}\text{-}6) + a_3 (\mathbf{M}\text{-}6)^2 + a_4 \log R + a_5 R \qquad (8)$$

where $R=\sqrt{(D^2 + h^2)}$, D is the closest distance to the fault (or hypocentral distance for small events) and h is given by $\log h = 0.05 + 0.15\ \mathbf{M}$. Table 4 gives the coefficients of the relations for each type of event. Note that for offshore events, the coefficients are the same as for crustal events, but the terms (**M**-6) in Equation 8 are replaced by (**M**-6.5) to produce the required 0.5 magnitude unit offset for such events.

The fit of the relations to data is more critical for the larger magnitudes of more relevance to hazard estimation. The fit is examined in various magnitude ranges in Figures 12 through 14, which plot the residuals (log observed PSA – log predicted PSA) versus distance by magnitude range for crustal, in-slab and offshore events, respectively. Both vertical-component data (*H/V) and horizontal-component data are included. Soil data are included in most cases, using the empirical soil response factors of Abrahamson and Silva (1997) to predict soil motions. However, in Figure 13 the soil data from the Nisqually earthquake are not included. The soil data from Nisqually were gathered in the Puget Sound region, and are believed to include particularly high site response due to basin effects (Frankel et al., 1999, 2002; Atkinson and Casey, 2003). The generic soil amplification factors of Abrahamson and Silva (1997) will not adequately model these effects, resulting in bias. From these figures, I conclude that the developed ground-motion relations of Table 4 provide a reasonable fit to the Cascadia data for $\mathbf{M} \geq 5$, while overestimating the response spectra from smaller events. For the offshore events, the amplitudes are greatly overpredicted beyond 200 km, as offshore attenuation becomes steeper in this distance range, but this is not very significant for hazard analysis. If desired, the offshore attenuation rate could be made steeper to accommodate this feature. Thus the developed hybrid-empirical ground-motion relations are a suitable basis for seismic hazard estimation in the Cascadia region, for crustal, in-slab and offshore events.

Figure 15 compares the developed relations for crustal and in-slab Cascadia earthquakes to those for other regions, in particular to empirical relations for California (Abrahamson and Silva, 1997) and for the in-slab relations developed from a global subduction database by Atkinson and Boore (2003) and by Youngs et al. (1997), all for rock sites. Cascadia ground motions for crustal events are slightly less than those for California crustal events. For in-slab events, the relations suggested by this study are similar to those predicted by Atkinson and Boore (2003) from the global database, but predict lower amplitudes (as much as a factor of 2) directly above the source. The Atkinson and Boore (2003) relations may be more reliable in this case due to the larger global database at short distances. The earlier in-slab relations of Youngs et al. (1997)

are commonly used, but are weak in data. The discrepancies observed between the relations serve as a measure of epistemic uncertainty in amplitudes.

Uncertainty in Ground Motion Relations

An important issue for the use of ground-motion relations in seismic hazard analysis concerns their uncertainty. Two types of uncertainty are important: epistemic uncertainty, representing our uncertainty in the correctness of the median, and aleatory uncertainty, representing random variability of observations about the median (Toro and McGuire, 1987). An estimate of the epistemic uncertainty can be obtained by examining Figures 12 through 16. Given the differences between these relations and those for other regions, the discrepancies between the developed relations and data, and our uncertainty in the statement that the source parameters are equivalent across regions, the median relations for events of **M**>5 could be adjusted by as much as +/- a factor of 1.5 to 2 and still be consistent with regional data and other considerations. The regional attenuation with distance is well-constrained beyond 40 km, but there is the possibility that attenuation of crustal events within 40 km could differ significantly from that in California. This requires further study with new data and is difficult to quantify at this time.

The aleatory uncertainty can be represented by the standard deviation of the residuals (sigma). This is the total aleatory uncertainty, representing both inter-event and intra-event components. Figure 16 plots this variability versus magnitude for Cascadia events in comparison to typical values for California, as given by Abrahamson and Silva (1997) (upper part of the figure). The mean residuals averaged in magnitude ranges are also plotted (lower part of the figure). The large negative mean residuals in Figure 16 are potentially misleading in some cases, as the residuals tend to decrease at greater distances. Looking at just the limited data for events of **M**≥5 at R≤100 km, the mean residuals for 1 Hz are -0.18, +0.14 and -0.24 for crustal, in-slab and offshore events, respectively; for 5 Hz the mean residuals are -0.15, +0.23, and -0.40, respectively. Thus for these cases (**M**≥5 at R≤100 km), mean residuals indicate an error of less than a factor of two overall.

Based on the lack of data for Cascadia at close distances, and the fact that the overall trend in standard deviations appears to follow that suggested for California, I suggest that aleatory uncertainty should be assumed to equal that for California (eg. as given in Abrahamson and Silva, 1997). It is a reasonable assumption that variability in amplitudes should be similar in the two regions, since they are driven by the same gross factors (random variability in earth properties, directivity, etc.). On the other hand, it is also possible that variability of ground motion is greater in Cascadia due to the complicated crustal and subcrustal geometry of the subduction zone through which the waves travel.

In summary, in applying the hybrid-empirical ground-motion relations of Table 3, I suggest an overall epistemic uncertainty of a factor of 1.5 to 2, with aleatory uncertainty given by the California sigma values of Abrahamson and Silva (1997).

CONCLUSIONS

A simple application of the hybrid-empirical approach is well-suited to the development of regional ground-motion relations for earthquakes in the Cascadia region of southwestern British Columbia and northwestern Washington. Separate ground-motion relations are developed for crustal, in-slab and offshore events. For crustal earthquakes in Cascadia, ground motions are obtained by multiplying California ground-motion relations by a frequency-dependent factor to account for regional differences in crustal amplification. The ground motion from offshore events can be predicted by using the Cascadia crustal relations, but for one-half moment magnitude unit less (eg. predict **M**7 motions using relations for **M**6.5). In-slab earthquakes attenuate more rapidly with distance (R) than do crustal earthquakes. Their ground motions are predicted by multiplying Cascadia crustal relations by the factor 1.17 exp(-0.004 R). The developed ground-motion relations for Cascadia earthquakes are in reasonable agreement with recorded ground motions in the region.

STUDY PUBLICATIONS

The publication by Atkinson and Boore (2003), cited below, was completed as part of this research program. The material presented in this report is also being submitted to Bull. Seism. Soc. Am. under the same title as this report (projected publication date 2005). The compiled Fourier spectra and response spectra datafiles are available in electronic format by sending a request to gmatkinson@aol.com.

REFERENCES

Abrahamson, N. and W. Silva (1997). Empirical response spectral attenuation relations for shallow crustal earthquakes. Seism. Res. L., **68**, 94-127.

Adams, J., and Halchuk, S. (2003). Fourth generation seismic hazard maps of Canada: Values for over 650 Canadian localities intended for the 2005 National Building Code of Canada. Geological Survey of Canada Open File 4459 150 pp.

Atkinson, G. (1995). Attenuation and source parameters of earthquakes in the Cascadia region. Bull. Seism. Soc. Am., **85**, 1327-1342.

Atkinson, G. (2001). An alternative to stochastic ground motion relations for use in seismic hazard analysis in eastern North America. Seism. Res. L., **72**, 299-306.

Atkinson, G. (2004). Empirical attenuation of ground motion spectral amplitudes in southeastern Canada and the northeastern United States. Bull. Seism. Soc. Am.,submitted.

Atkinson, G., and D. Boore (1997). Stochastic point-source modeling of ground motions in the Cascadia region. Seism. Res. L., **68**, 74-85.

Atkinson, G. and D. Boore (2003). Empirical ground-motion relations for subduction zone earthquakes and their application to Cascadia and other regions. Bull. Seism. Soc. Am., **93**, 1703-1729.

Atkinson, G. and R. Casey (2003). A comparison of ground motions from the 2001 M6.8 in-slab earthquakes in Cascadia and Japan. Bull. Seism. Soc. Am.,**93,** 1823-1831.

Atkinson, G. and J. Cassidy (2000). Integrated use of seismograph and strong motion data to determine soil amplification in the Fraser Delta: results from the Duvall and Georgia Strait earthquakes. Bull. Seism. Soc. Am., **90**, 1028-1040..

Atkinson, G. and S. McCartney (2004). A revised magnitude-recurrence relation for shallow crustal earthquakes in southwestern British Columbia, considering the relationship between moment magnitude and regional magnitude scales. Bull. Seism. Soc. Am., submitted.

Atkinson, G. and R. Mereu (1992). The shape of ground motion attenuation curves in southeastern Canada. Bull. Seism. Soc. Am., **82**, 2014-2031.

Atkinson, G. and W. Silva (2000). Stochastic modeling of California ground motions. Bull. Seism. Soc. Am., **90**, 255-274.

Atkinson, G. and W. Silva (1997). Empirical source spectra for California earthquakes. Bull. Seism. Soc. Am., **87**, 97-113.

Beresnev, I. and G. Atkinson (1997). Shear wave velocity survey of seismographic sites in eastern Canada: Calibration of empirical regression method of estimating site response. Seism. Res. L., **68**, 981-987.

Boore, D. (1983). Stochastic simulation of high-frequency ground motions based on seismological models of the radiated spectra. Bull. Seism. Soc. Am., **73**, 1865-1894.

Boore, D. and W. Joyner (1997). Site amplifications for generic rock sites. Bull. Seism. Soc. Am., **87**, 327-341.

Brune, J. (1970). Tectonic stress and the spectra of seismic shear waves from earthquakes. J. Geophys. Res., **75**, 4997-5009.

Burger, R., P. Somerville, J. Barker, R. Herrmann, and D. Helmberger (1987). The effect of crustal structure on strong ground motion attenuation relations in eastern North America. Bull. Seism. Soc. Am., **77**, 420-439.

Campbell, K. (2003). Prediction of strong-ground motion using the hybrid-empirical method and its use in the development of ground-motion (attenuation) relations in eastern North America. Bull. Seism. Soc. Am., **93,** 1012-1033.

Chen, S. and G. Atkinson (2002). Global comparisons of earthquake source spectra. Bull. Seism. Soc. Am., **92**, 885-895.

Frankel, A., Carver, D., Cranswick, E., Meremonte, M., Bice, T., & Overturf, D. (1999) "Site response for Seattle and source parameters of earthquakes in the Puget Sound region" *Bull. Seis. Soc. Am.* **89, 2** 468-483.

Frankel, A., D. Carver and R. Williams (2002). Nonlinear and linear site response and basin effects in Seattle for the **M** 6.8 Nisqually, Washington, earthquake. Bull. Seism. Soc. Am., **92**, 2090-2109.

Frankel, A., C. Mueller, T. Barnhard, D. Perkins, E. Leyendecker, N. Dickman, S. Hopper and M. Hopper (1996). National seismic hazard maps, June 1996. U.S.G.S. Open-file Rpt. 96-532.

Frankel, A., C. Mueller, T. Barnhard, D. Perkins, E. Leyendecker, N. Dickman, S. Hanson and M. Hopper (1999). National seismic hazard mapping project. http://geohazards.cr.usgs.gov

Herrmann, R. and L. Malagnini (2004). Interpretation of high frequency ground motion from regional seismic network observations. Bull. Seism. Soc. Am., draft manuscript.

Hyndman, R., G. Rogers, D. Dragert, K. Wang, J. Clague, J. Adams and P. Bobrowsky (1996). Giant earthquakes beneath Canada's west coast. Geoscience Canada, **23**, 2, 63-72.

Joyner, W. and D. Boore (1993). Methods for regression analysis of strong-motion data. Bull. Seism. Soc. Am., **83**, 469-487.

Joyner, W.B. and D.M. Boore (1994). Errata, Bull. Seism. Soc. Am., **84**, 955-956.

Lermo, J. and F. Chavez-Garcia (1993). Site effect evaluation using spectral ratios with only one station. Bull. Seism. Soc. Am., **83**, 1574-1594.

Motazedian, D. and G. Atkinson (2004). Region-specific ground motion relations for Puerto Rico. Active tectonics and seismic hazards of Puerto Rico, the Virgin Islands and offshore areas. Special GSA Issue, in press.

Raoof, M., R. Herrmann and L. Malagnini (1999). Attenuation and excitation of three-component ground motion in sourthern California. Bull.Seism. Soc. Am., **89**, 888-902.

Ristau, J. (2004). Seismotectonics of western Canada from regional moment tensor analysis. Ph.D. Dissertation. School of Earth and Ocean Sciences. University of Victoria, Victoria, B.C.

Ristau, J., G. Rodgers and J. Cassidy (2003). Moment magnitude-Local magnitude calibration for earthquakes off Canada's west coast. Bull. Seism. Soc. Am., **93**, 2296-2300.

Siddiqqi, J. and G. Atkinson (2002). Ground motion amplification at rock sites across Canada, as determined from the horizontal-to-vertical component ratio. Bull. Seism. Soc. Am., **92**, 877-884.

Toro, G. and R. McGuire (1987). Calculational procedures for seismic hazard analysis and its uncertainty in the eastern United States. Proc. Third Intl. Conf. Soil Dynamics and Earthquake Eng., Princeton, pp. 195-206.

Youngs, R., S. Chiou, W. Silva and J. Humphrey (1997). Strong ground motion attenuation relationships for subduction zone earthquakes. Seism. Res. L., **68**, 58-73.

Table 1: List of earthquakes of M>4 with PSA data at R<300 km

Notes: nrec= number of records, it=1 for crust, 2 for in-slab, 3 for offshore

day	mo	year	nrec	it	depth(km)	**M**
13	4	1949	4	2	54	6.8
29	4	1965	8	2	60	6.7
14	2	1981	3	1	7	5.3
16	6	1986	8	2	35	5.4
5	3	1989	17	2	46	4.5
18	6	1989	13	2	45	4.4
12	9	1989	15	2	34	4.5
24	12	1989	4	1	18	4.3
2	4	1990	17	1	1	4.5
14	4	1990	17	1	2	4.8
25	4	1992	30	1	11	7.1
21	9	1993	2	1	6	6.0
3	1	1994	12	2	28	5.7
3	5	1996	17	1	4	5.1
25	6	1998	3	3	10	5.3
30	8	1998	6	3	10	5.3
30	8	1998	4	2	4	6.2
1	9	1998	4	2	6	4.6
3	7	1999	20	2	41	5.8
11	12	1999	19	2	53	4.9
30	4	2000	16	3	10	5.4
15	5	2000	13	3	10	5.3
15	5	2000	12	3	10	5.3
10	6	2000	12	3	10	5.0
1	8	2000	22	2	41.3	4.9
11	1	2001	9	3	10	6.0
23	1	2001	10	3	10	5.5
23	1	2001	17	3	10	5.7
17	2	2001	7	3	20	5.0
17	2	2001	7	3	20	5.3
17	2	2001	7	3	20	6.3
28	2	2001	164	2	52	6.8
7	4	2001	20	2	32.1	4.2
10	4	2001	9	3	10	5.3
2	5	2001	6	3	10	5.4
10	6	2001	15	2	44.6	5.0
22	7	2001	8	2	50.3	4.1
20	10	2001	23	2	38.3	4.1
20	2	2002	14	3	10	5.1
17	8	2002	32	1	10	4.5
5	9	2002	10	3	20	5.2
21	9	2002	42	1	26.2	4.3

day	mo	year	nrec	it	depth(km)	**M**
30	10	2002	9	3	20	5.0
3	11	2002	12	3	10	5.8
25	4	2003	50	2	51.3	4.6
1	7	2003	20	3	10	5.0
19	12	2003	15	3	10	5.4
17	3	2004	58	1	1.3	4.2

Table 2 - Coefficients of regression (Equations 1, 5)

f(Hz)	c1	c2	c3	b	t	c4
crust				**rt1 = 90 km**		**rt2= 300 km**
0.50	-1.893	1.564	0.1185	-0.447	-0.293	-0.00078
0.63	-1.446	1.589	-0.0219	-0.550	-0.306	-0.0009
0.79	-0.361	1.587	-0.0547	-1.047	-0.056	-0.0013
1.00	0.128	1.548	-0.1141	-1.222	0.170	-0.0018
1.26	0.245	1.485	-0.1501	-1.152	0.048	-0.0022
1.59	0.123	1.475	-0.1229	-0.992	0.071	-0.0026
2.00	0.033	1.396	-0.0713	-0.872	-0.001	-0.0029
2.51	0.024	1.301	-0.1052	-0.790	-0.175	-0.0031
3.16	0.159	1.186	-0.1048	-0.821	-0.355	-0.0032
3.98	0.588	1.065	-0.1570	-1.017	-0.389	-0.0034
5.01	0.475	1.027	-0.2216	-0.930	-0.683	-0.0034
6.31	0.548	0.975	-0.1538	-0.961	-0.996	-0.0033
7.94	0.440	0.916	-0.1050	-0.933	-1.145	-0.0034
10.00	0.505	0.847	-0.0625	-0.981	-1.323	-0.0035
12.59	0.779	0.805	0.0327	-1.188	-1.813	-0.0027
15.85	1.022	0.685	-0.1662	-1.378	-3.137	-0.0013
19.95	0.750	0.673	0.2463	-1.349	-3.865	-0.00044
In-slab				**rt1 = 120 km**		**rt2=170**
0.50	0.066	1.269	0.4493	-1.373	-1.215	-0.00078
0.63	-0.403	1.571	-0.0434	-1.027	-1.181	-0.0009
0.79	-0.523	1.646	-0.2225	-0.884	-0.986	-0.0013
1.00	0.088	1.591	-0.2060	-1.085	-0.811	-0.0018
1.26	0.418	1.517	-0.2137	-1.136	-0.941	-0.0022
1.59	0.895	1.501	-0.2625	-1.303	-0.564	-0.0026
2.00	1.145	1.490	-0.3006	-1.384	-0.383	-0.0029
2.51	1.339	1.421	-0.3416	-1.436	-0.365	-0.0031
3.16	1.116	1.367	-0.3540	-1.315	-0.567	-0.0032
3.98	1.349	1.372	-0.3939	-1.418	-0.446	-0.0034
5.01	1.879	1.326	-0.4089	-1.706	-0.344	-0.0034
6.31	2.364	1.281	-0.4093	-1.968	-0.640	-0.0033
7.94	2.275	1.226	-0.3067	-1.951	-0.865	-0.0034
10.00	2.646	1.264	-0.4069	-2.151	-0.771	-0.0035
12.59	2.652	1.202	-0.3462	-2.248	-1.190	-0.0027
15.85	2.553	1.286	-0.3889	-2.311	-3.920	-0.0013
19.95	2.764	1.145	-0.3463	-2.520	-4.891	-0.00044

f(Hz)	c1	c2	c3	b	t	c4
Offshore				**rt1=140 km**		**rt2=260 km**
0.50	-1.842	1.397	-0.0284	0.033	-1.980	-0.00078
0.63	-1.439	1.447	-0.0874	-0.118	-2.179	-0.0009
0.79	-0.971	1.480	-0.0983	-0.272	-2.130	-0.0013
1.00	-0.706	1.496	-0.0376	-0.330	-2.056	-0.0018
1.26	-0.262	1.453	-0.0173	-0.512	-1.828	-0.0022
1.59	-0.423	1.413	-0.0235	-0.382	-1.903	-0.0026
2.00	0.007	1.363	-0.0114	-0.577	-1.780	-0.0029
2.51	0.106	1.302	0.0015	-0.600	-1.909	-0.0031
3.16	0.183	1.250	0.0311	-0.646	-2.006	-0.0032
3.98	0.698	1.190	0.0314	-0.899	-1.948	-0.0034
5.01	1.034	1.127	0.0334	-1.073	-2.196	-0.0034
6.31	1.142	1.091	0.0498	-1.149	-2.400	-0.0033
7.94	1.509	1.082	0.0728	-1.342	-2.442	-0.0034
10.00	1.756	1.021	0.0679	-1.497	-2.397	-0.0035
12.59	2.350	0.944	0.0928	-1.887	-2.886	-0.0027
15.85	2.372	0.896	0.1038	-2.026	-3.898	-0.0013
19.95	1.768	0.802	0.0795	-1.885	-4.847	-0.00044

Table 3 – Multiplicative Factors to obtain Cascadia ground motions from California ground motion relations

Notes: FC(CA) is the crustal and anelastic attenuation factor for California (soft rock site), FC(BC) is the corresponding factor for the Cascadia region (hard rock site in B.C.), and the resulting factor to apply is FC(BC)/FC(CA)

Freq(Hz)	FC(CA)	FC(BC)	FC(BC)/FC(CA)
0.1	1.12	1.0	0.892
0.5	1.32	1.08	0.818
0.8	1.46	1.11	0.760
1.0	1.52	1.13	0.743
2.0	1.61	1.17	0.727
3.0	1.57	1.19	0.758
5.0	1.40	1.21	0.864
8.0	1.12	1.21	1.08
10.	0.96	1.21	1.26
20.	0.40	1.13	2.82

Table 4 – Regression Coefficients for Cascadia ground-motion relations (Equation8)

f(Hz)	a1	a2	a3	a4	a5
Crust (and offshore with adjustment to M in Equation 8)					
0.1	1.4172	0.9466	-0.0587	-1.0116	
0.2	2.0247	0.8884	-0.0809	-1.0109	
0.32	2.2116	0.8628	-0.0886	-1.0179	
0.5	2.5913	0.7957	-0.1069	-1.0341	
1	3.1283	0.6818	-0.1158	-1.0925	-0.0002
2	3.5520	0.5615	-0.1031	-1.0977	-0.0013
3.2	3.8160	0.4907	-0.0844	-1.1309	-0.0020
5	4.0439	0.4356	-0.0626	-1.1721	-0.0028
10	4.3732	0.3972	-0.0413	-1.2977	-0.0035
20	4.6827	0.4064	-0.0378	-1.4813	-0.0018
pga	3.9427	0.4182	-0.0446	-1.4070	-0.0014
pgv	2.3557	0.5796	-0.0338	-1.2450	
In-slab					
0.1	1.6507	0.9526	-0.0585	-1.1852	-0.0001
0.2	2.2214	0.8931	-0.0807	-1.1458	-0.0005
0.32	2.3941	0.8669	-0.0885	-1.1379	-0.0006
0.5	2.7057	0.7974	-0.1068	-1.0826	-0.0013
1	2.7057	0.7974	-0.1068	-1.0826	-0.0013
2	3.6202	0.5615	-0.1031	-1.0977	-0.0030
3.2	3.8841	0.4907	-0.0844	-1.1309	-0.0037
5	4.1121	0.4356	-0.0626	-1.1721	-0.0046
10	4.4414	0.3972	-0.0413	-1.2977	-0.0052
20	4.7509	0.4064	-0.0378	-1.4813	-0.0035
pga	4.0109	0.4182	-0.0446	-1.4070	-0.0032
pgv	2.5341	0.5835	-0.0336	-1.3607	-0.0007

Note: Recommended value for total standard error (sigma) is that given by Abrahamson and Silva (1997), as shown on Figure 16. For soil sites, the soil response coefficients as given by Abrahamson and Silva (1997) may be used.

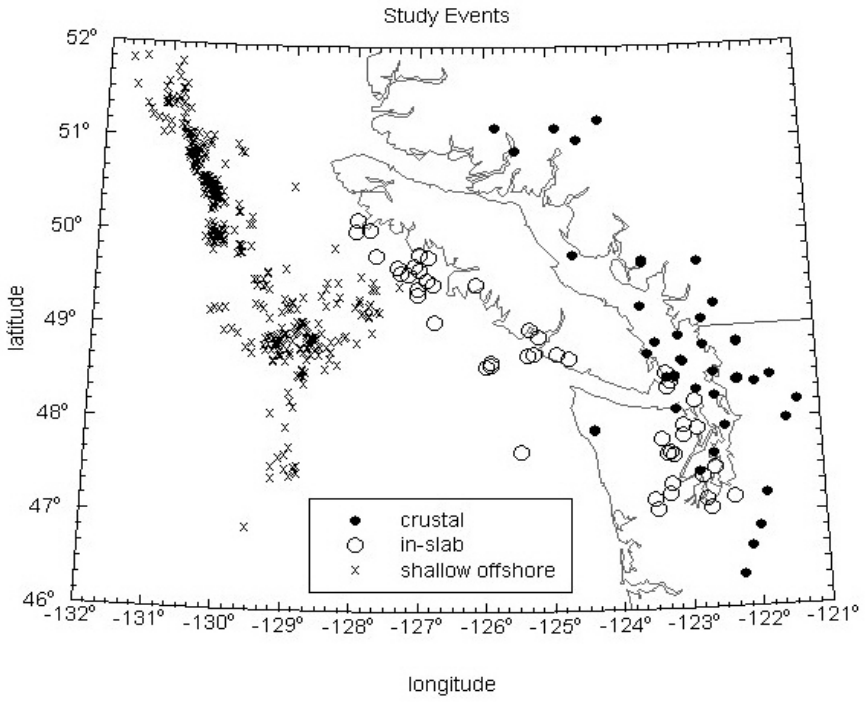

Figure 1 – Location of study events, showing crustal (filled circles), in-slab (open circles) and offshore (x) events.

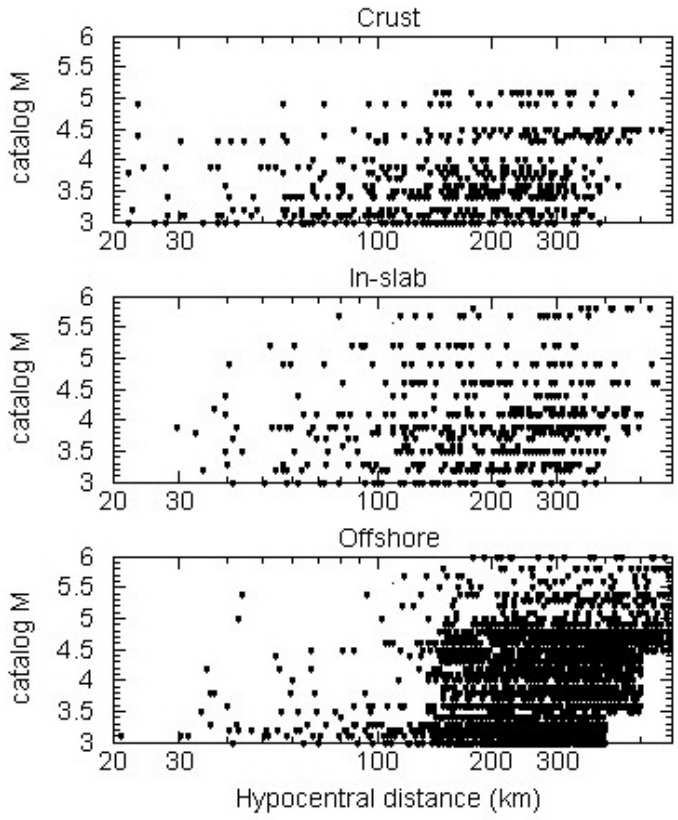

Figure 2 – Distribution of Fourier spectra database in magnitude and distance for crustal (top), in-slab (middle) and offshore events (lower).

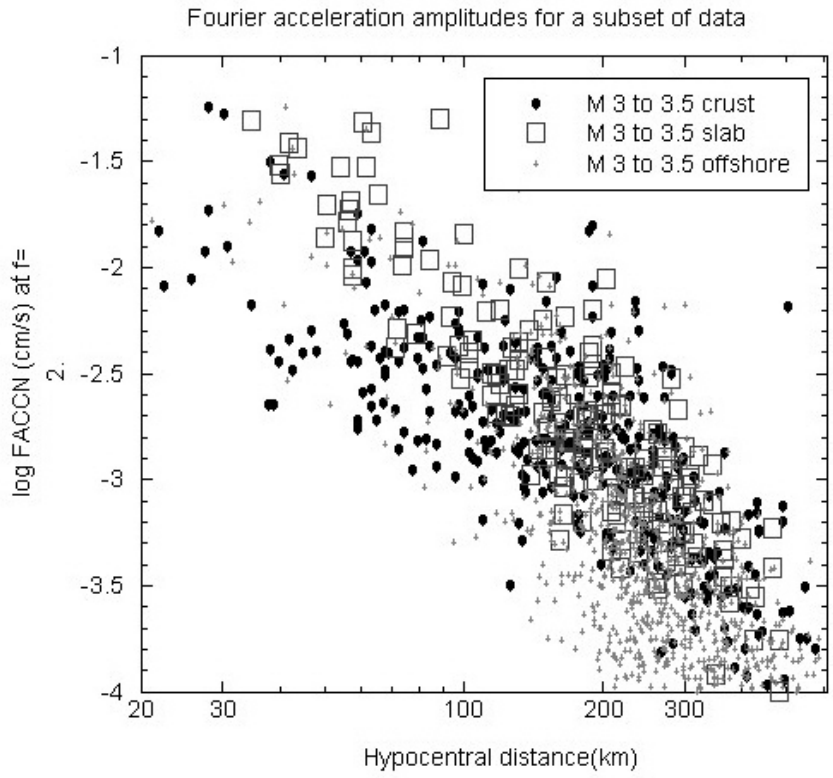

Figure 3 – Fourier spectral amplitudes (f=2 Hz) for earthquakes of catalog magnitude 3.0 to 3.5.

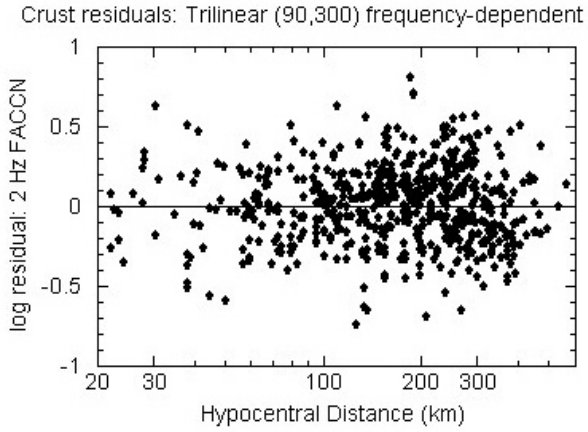

Figure 4 – Example of residuals (2 Hz) versus distance for crust dataset (vertical component), for trilinear frequency-dependent regression.

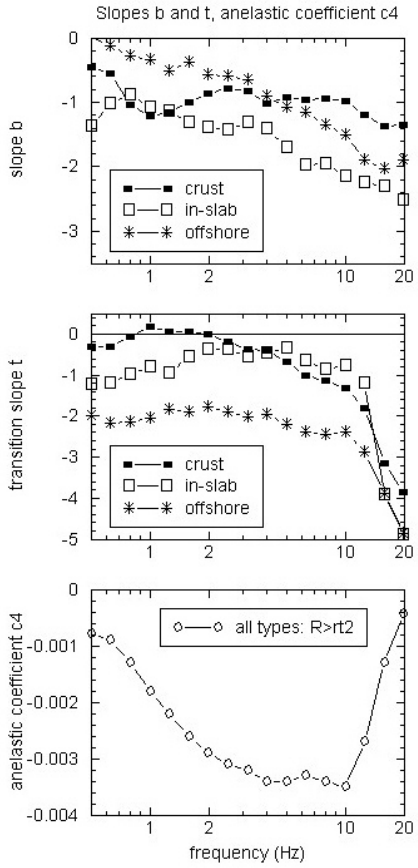

Figure 5 – Attenuation coefficients for trilinear regression, showing attenuation slopes *b* (for $R \leq r_{t1}$) (top) and *t* (for $r_{t1} < R \leq r_{t2}$) (middle) and anelastic coefficient c_4 (lower).

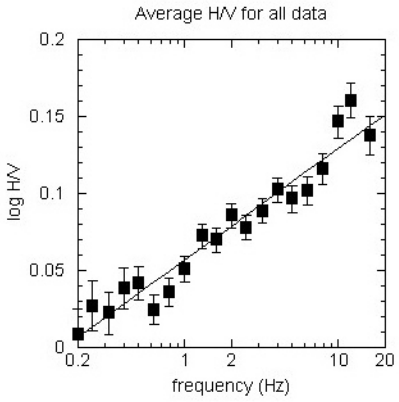

Figure 6 – Mean value of log H/V (horizontal-to-vertical component ratio). Symbols show mean and standard error. Line shows best fit by least-squares.

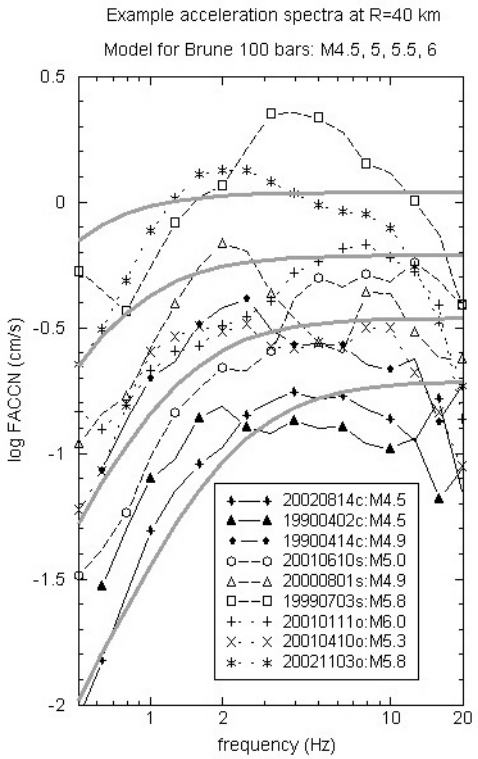

Figure 7 – Example of acceleration spectra at reference distance of 40 km for several events of **M** 4.5 to 6 (lines with symbols), in comparison to Brune model spectra with 100 bar stress drop (smooth lines) for **M** 4.5, 5.0, 5.5 and 6.0. Event legend gives date and moment magnitude of event: c=crustal, s=in-slab, o=offshore.

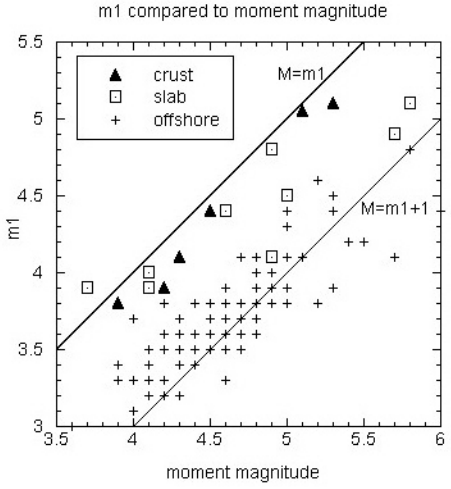

Figure 8 – m1 as determined for events in this study versus moment magnitude, as determined by Ristau (2004). Lines show relationships **M** = m1 and **M** =m1+1 for reference.

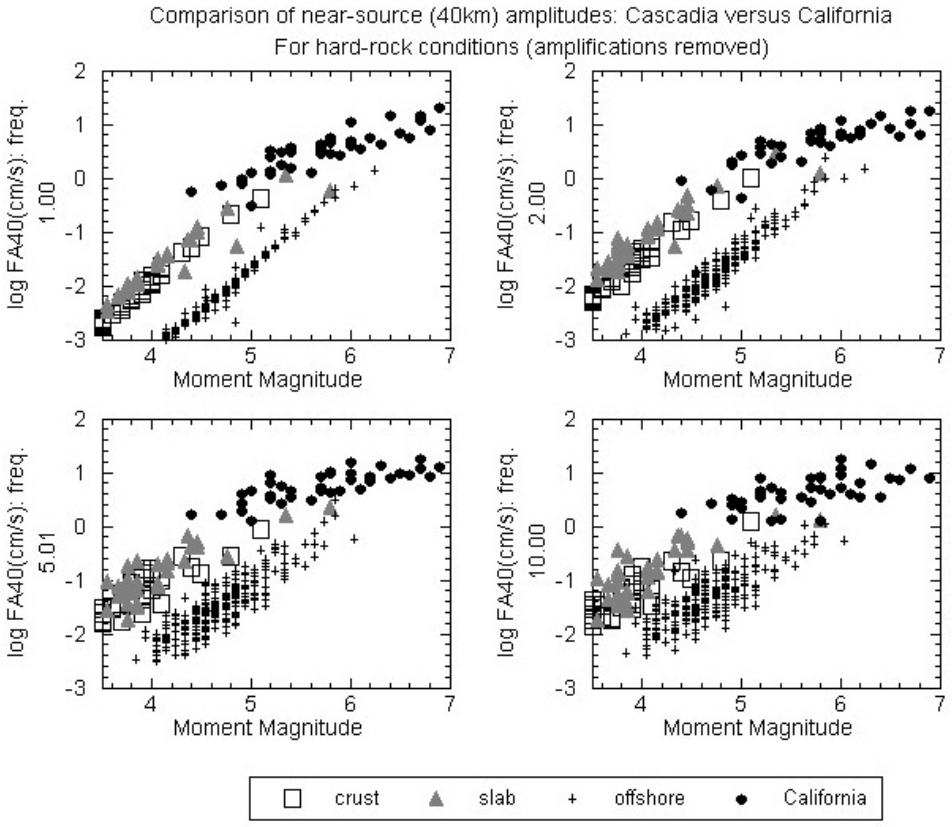

Figure 9 – Comparison of Fourier amplitudes at reference distance of 40 km, for hard-rock conditions (all amplifications removed), for California and Cascadia events, for frequencies of 1, 2, 5 and 10 Hz.

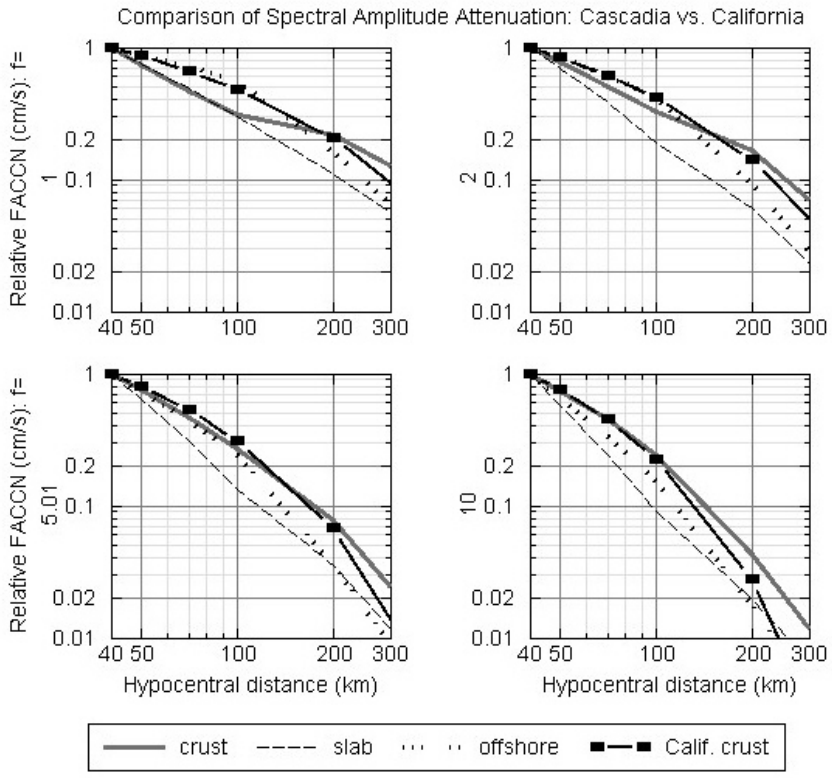

Figure 10 – Relative attenuation of Fourier amplitudes for California crustal events (line with symbols) compared to Cascadia events (lines), for frequencies 1, 2, 5 and 10 Hz.

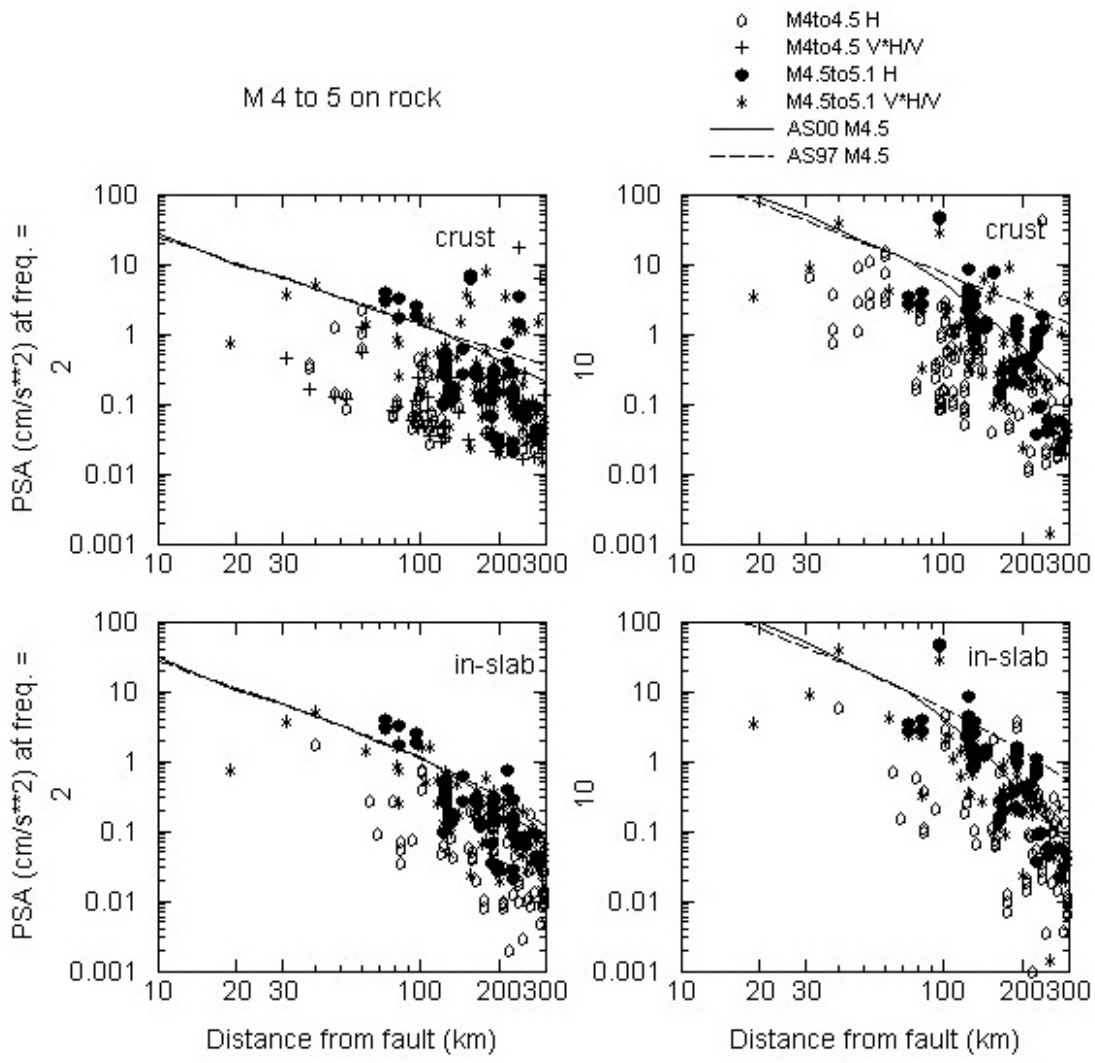

Figure 11 – Observed PSA for Cascadia events of **M** 4 to 5 compared to proposed ground-motion relations for **M** 4.5, for 2 and 10 Hz. Top panels are crustal events, lower panels are in-slab events. Symbols distinguish events at high and low end of magnitude range, and distinguish horizontal components from vertical components multiplied by H/V ratio.

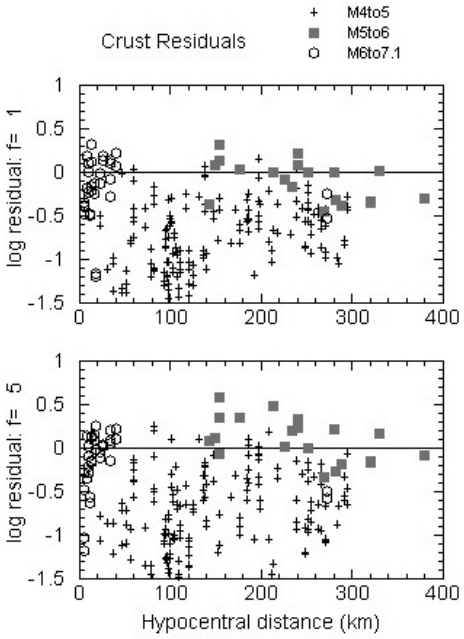

Figure 12 – PSA residuals for proposed ground-motion relations for crustal events at 1 and 5 Hz. Symbols distinguish magnitude ranges of data.

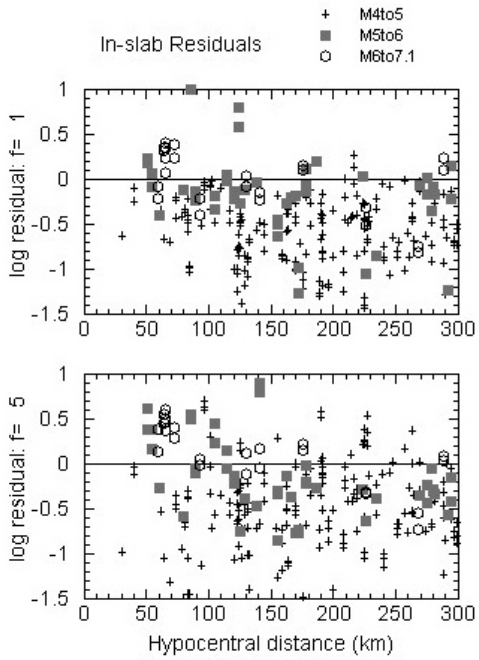

Figure 13 – PSA residuals for proposed ground-motion relations for in-slab events at 1 and 5 Hz. Symbols distinguish magnitude ranges of data.

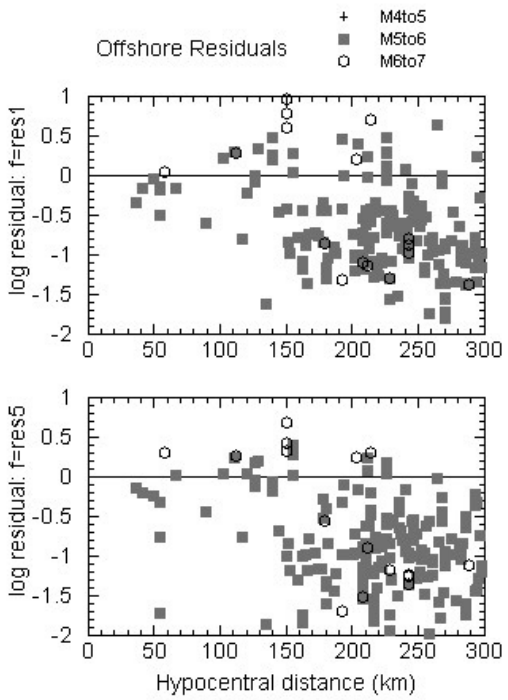

Figure 14 – PSA residuals for proposed ground-motion relations for offshore events at 1 and 5 Hz. Symbols distinguish magnitude ranges of data.

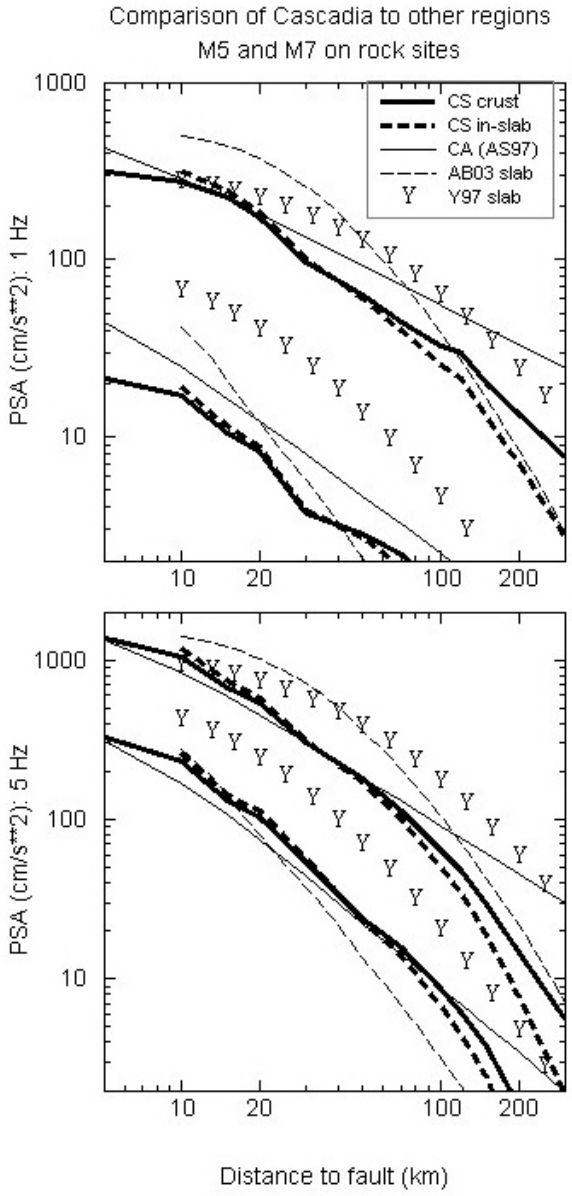

Figure 15 – Comparison of Cascadia ground-motion relations (heavy lines) with those of Abrahamson and Silva (1997) for California (light solid line), Atkinson and Boore (2003) for in-slab events (global database, light dashed line) and Youngs et al. (1997) in-slab events (Y), for 1 and 5 Hz PSA, for events of **M** 5 and 7 on rock.

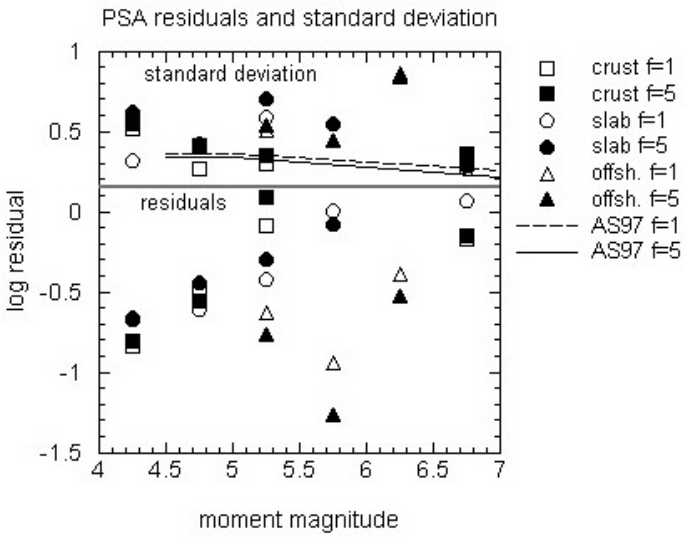

Figure 16 – Mean PSA residuals (plotted below line) and their standard deviations (plotted above line) for crust, in-slab and offshore events at 1 and 5 Hz. Lines show California standard deviations of Abrahamson and Silva (1997).